Emergence of the Shackleton Range from beneath the Antarctic Ice Sheet due to glacial erosion

Emergence of the Shackleton Range from beneath the Antarctic Ice Sheet due to glacial erosion

D.E. Sugden,[a] C. J. Fogwill,[b] A. S. Hein,[a] F. M. Stuart,[c] A. R. Kerr,[a] P. W. Kubik [d]

[a] School of GeoSciences, University of Edinburgh, Drummond Street, Edinburgh, EH8 9XP, UK.
[b] Climate Change Research Centre, School of Biological Earth and Environmental Sciences, University of New South Wales, Sydney, Australia.
[c] Scottish Universities Environmental Research Centre, Rankine Avenue, East Kilbride, G75 0QF, UK.
[d] Laboratory of Ion Beam Physics, ETH Zurich, 8093, Zurich, Switzerland.

Abstract

This paper explores the long-term evolution of a subglacial fjord landscape in the Shackleton Range, Antarctica. We propose that prolonged ice-sheet erosion across a passive continental margin caused troughs to deepen and lower the surrounding ice-sheet surface, leaving adjacent mountains exposed. Geomorphological evidence suggests a change in the direction of regional ice flow accompanied emergence. Simple calculations suggest that isostatic compensation caused by the deepening of bounding ice-stream troughs lowered the ice-sheet surface relative to the mountains by ~ 800 m. Use of multiple cosmogenic isotopes on bedrock and erratics (^{26}Al, ^{10}Be, ^{21}Ne) provides evidence that overriding of the massif and the deepening of the adjacent troughs occurred earlier than the Quaternary. Perhaps this occurred in the mid-Miocene, as elsewhere in East Antarctica in the McMurdo Dry Valleys and the Lambert basin. The implication is that glacial erosion instigates feedback which can change ice-sheet thickness, extent and direction of flow. Indeed, as the sub-glacial troughs evolve over millions of years, they increase topographic relief and this changes the dynamics of the ice sheet.

Key words

Antarctic Ice Sheet fjord evolution glacial erosion cosmogenic nuclides Shackleton Range passive margin

Corresponding author: David E. Sugden. Tel (44) 0131 663 7605 email: david.sugden@ed.ac.uk

1. Introduction

We explore the long-term evolution of the Shackleton Range, a massif in the Weddell Sea sector of the Transantarctic Mountains (Fig. 1). The massif is bounded by the Slessor and Recovery outlet glaciers which drain the East Antarctic Ice Sheet. If deglaciated the massif would comprise a fjord landscape, with Slessor and Recovery glaciers now filling troughs excavated below sea level. Fjord landscapes in the Northern Hemisphere are characteristic of passive continental margins bounding the North Atlantic and are especially well developed in Norway (Holtedahl, 1967), northeast Greenland (Bretz, 1935) and Baffin Island (Løken and Hodgson, 1971). Here most fjords exploit pre-existing river valleys and dissect relatively flat uplands. Their origin is thought to primarily reflect interplay between ice-sheet dynamics and topography (Kessler *et al*., 2008), while their morphology is also affected by the pattern of both basal thermal regime (Briner *et al.*, 2008; Kleman *et al.*, 2008) and rock strength (Augustinus, 1992; Swift *et al.*, 2008). In the Northern Hemisphere, the interpretation of long-term evolution is based mainly on inferences from landscape form. The advantages of studying such a landscape in the Antarctic is both that the glacial processes are there to see and that there is a long history of ice-sheet glaciation extending back tens of millions of years, rather than the shorter glacial episodes of the Northern Hemisphere.

There is a long-held view that the erosion of troughs through passive continental margins leads to the progressive emergence of intervening uplands from beneath an ice sheet. The transition from dissected coastal mountains to inland plateau landscapes around existing and former Northern Hemisphere ice sheets has been interpreted as showing that, during the course of glaciation, outlet glaciers establish lower and shallower ice-sheet surface gradients as they deepen and extend their troughs (eg. Fig. 10.12 in Sugden and John, 1976). The deeper the trough and the more it extends inland, the lower the resulting ice sheet surface will be and the greater the extent of exposed surrounding uplands. In many locations, and indeed in the Shackleton Range, local plateau ice caps can build up on the exposed mountains. A contributing factor to emergence is isostatic recovery achieved as a result of the substitution of the rock volume of a trough by less dense ice. This latter process can account for the uplift of adjacent massifs by hundreds of metres (Kerr and Gilchrist, 1996; Stern *et al.*, 2005; Jamieson *et al.*, 2008). A further implication is that the process of erosion itself introduces feedbacks which affect the dynamics of the ice sheet, even its oscillations (Tomkin, 2003; Hein *et al.*, 2011).

In view of the interaction of ice sheets with independent tectonic, sea-level and climatic controls, it is difficult to quantify the role of glacial erosion in the emergence of uplands. However, there is evidence elsewhere in East Antarctica of ice in mountainous areas that was thicker at an early stage and this can be interpreted as partly reflecting rock exposure as a result of glacial erosion. For example, an ice sheet roughly 1000 m thicker than present overrode the topography of the Dry Valleys and Convoy mountain blocks in southern Victoria Land (Sugden and Denton, 2004). $^{40}Ar/^{39}Ar$ ages of volcanic ashes suggest this occurred at ~14 Ma and the mountains have been largely free of an ice sheet since (Marchant *et al.*, 1993). Cosmogenic nuclide analyses in Queen Maud Land suggest that the mountains have emerged from beneath the ice sheet in the last 1-4 Ma (Altmaier *et al.*, 2010). Glaciomarine deposits on the flanks of the Lambert Glacier are pre-late Miocene and late Miocene in age and have been uplifted by 500 m and 200 m respectively (Hambrey *et al*., 2007). Further,

low temperature thermochronology has been used to argue that the Lambert trough was deepened 1.6-2.5 km during the early stages of Antarctic ice-sheet glaciation (Thomson *et al.*, 2013). It is possible that these landscape changes result from the lowering of the ice-sheet surface in response to the progressive deepening of adjacent glacial troughs, although other explanations cannot be ruled out. In the case of the Shackleton Range it is possible to isolate the role of glacier erosion with more confidence.

2. The Shackleton Range

The Shackleton Range is part of the Transantarctic Mountains that extends over 3000 km across Antarctica (Fig. 1 inset). The mountain block extends 200 km from east to west and 75 km from north to south (Fig. 2). The bounding Slessor Glacier to the north is 50 km wide and in places the bed is 2000 m below sea level (Fretwell *et al.* 2013). Recovery Glacier to the south is 70 km in width and in the vicinity of the western Shackleton Range, the trough is ~ 2000 m below sea level. The high velocities and low gradients of both glaciers have been argued to show that they currently flow on sediment (Bamber *et al*., 2006; Rippin *et al*., 2006). Local glaciers flow radially from an ice cap centred on the massif. There are numerous small wind-drift glaciers dotted on otherwise ice-free areas accumulating on the western lee slopes of topographic highs.

The Shackleton mountain block is eroded wholly into basement rocks, mainly shales, sandstones and gneiss (Höfle and Buggisch, 1995; Stephenson, 1966). This contrasts with most of the Transantarctic Mountains, including the adjacent blocks of Whichaway Nunataks to the south and the Theron Mountains to the north, which are capped by Beacon Supergroup sediments, mainly sandstones (Kerr *et al*., 2000). In common with most of the Transantarctic Mountains the gross morphology is of fault-bound mountain blocks with a coastal escarpment and a plateau surface which in the east disappears beneath the East Antarctic Ice Sheet. In the Shackleton Range the Read Mountains on the south-eastern flank of the massif at ~1800 m are the highest summits (see Fig 1 for location). The western front of the mountain block comprises an escarpment rising 700-800 m above the Filchner Ice Shelf. Offshore, beneath the ice shelf, is the Thiel trough with a depth of over 1500 m extending northwards to the Filchner trough in the Weddell Sea (Makinson and Nicholls, 1999). Water depths are 900 m within 25 km of the summit of Mt. Provender at 950 m, the northwest point of the range. This morphology is typical of a passive continental margin and erosion of the mountains would have followed continental break up which, in the case of this part of the Weddell Sea, began around 136 Ma (Rogenhagen *et al*., 2004).

In the Shackleton Range a suite of landforms can be used to reconstruct the fluvial landscape prior to glaciation. Figure 3 shows escarpments, surfaces, valleys and rectilinear slopes in the western part of the mountains. The highest ground, comprising the rolling upper slopes of the Read Mountains with elevations of 1800-1950 m, is to the south and east of the mapped area (Fig. 1). The geomorphology reveals remarkably flat surfaces north and west of the core uplands. The surfaces are cut across different rock types (Höfle and Buggisch, 1995). With increasing distance from the core upland, the surfaces narrow and give way to ridges, often with rectilinear slopes. Valleys, most occupied by glaciers, radiate out from the upland axis. There are dendritic patterns to the north and the slopes in less-glaciated areas in the northwest are commonly rectilinear in form. Sinuous convergent patterns in the

ice surface reflect subglacial valleys flowing south from the upland axis towards Recovery Glacier. In the northern oases of Mount Provender and Mount Skidmore are gently rolling slopes dotted with conical inselbergs, many of which rise cleanly above gentler slopes around them. This open landscape extends to the edge of Slessor Glacier where its elevation is only 240 m above sea level. All these features are typical of the erosion of a passive continental margin with mountain blocks eroded by fluvial processes and escarpments invigorated by a new base level as a result of rifting (Beaumont *et al*, 2000; Jamieson and Sugden, 2008). There are likely to have been river valleys originating in interior mountains and flowing to the coast between mountain blocks (Bo *et al.*, 2000; Rose *et al.*, 2013; Webb, 1994). In the Shackleton block the pattern of escarpments parallel to or linked to tributaries some tens of km inland suggests slope retreat from a river system which is graded to sea level, at least in its lower reaches. Thus we envisage that the mountains were bounded by two through river valleys, Slessor and Recovery, with wide floors close to sea level.

There is evidence of overriding ice covering the western Shackleton Range and flowing to the northwest (Fig. 3). This evidence includes striated rock surfaces in the Read Mountains at 1750 m and at Stephenson Bastion at 1600 m, roches moutonnées showing ice flow from the southeast on the plateau at Stephenson Bastion and the summit of Mt Provender itself (Kerr and Hermichen, 1999), and glacial erratics of exotic Beacon Sandstone found at 1780 m in the Read Mountains, 1600 m and 1785 m on Stephenson Bastion, and 1200 m on Flat Top, 23 km southeast of Mount Skidmore (Höfle and Buggisch,1995). Erratics on Stephenson Bastion include limestones unknown in the Shackleton range but which occur in the Pensacola Mountains to the south. The deposits on the upper surfaces are highly weathered with many clay-sized particles and a salt crust up to 2 cm thick and are comparable to surfaces in the Dry Valleys that are millions of years old (Höfle, 1980). Taken together, the orientation of the erosional forms and the presence of exotic erratics known to occur to the south support the notion that ice moved in a northwesterly direction across the summits of the Shackleton Range. The altitude of the features implies overriding ice with a thickness at least 650 m higher than the surface of the present Recovery Glacier.

3. Samples and methods

In an earlier pilot study Fogwill *et al*. (2004) used cosmogenic ^{10}Be and ^{26}Al concentrations in three bedrock samples, one with striations, to establish that there has been no significant burial of the samples for between 1.16 ± 0.10 Ma and 3.0 ± 0.3 Ma. The implication is that the overriding event occurred in the Pliocene or earlier. Here we increase the number of samples and have also carried out analysis of ^{21}Ne on the original samples.

The three pilot samples presented by Fogwill *et al.* (2004) were taken from escarpment tops at Stephenson Bastion and Mt. Provender (SB1/J29; SB2/J31; NL1/J22). Additional samples were collected at the time in the Read Mountains overlooking Recovery Glacier (Fig. 1); sample AC1/F2 was from a rock knoll on the broad escarpment to the south of Arkell Cirque, sample AC2/F2 from a ridge top near Eskola Cirque, and AC3/F3 from the summit slope of Bowen Cirque, an outlier of the Read Mountains (Fogwill *et al.*, 2004). All these bedrock surfaces are iron stained, deeply weathered and affected by *in situ* rock shattering. Eight further samples were taken from lower summits. Sample LH1/J15 is from a bedrock knoll on Lister

Heights, northwest of Fuchs Dome (Fig. 3). Two further samples were taken from the plateau surface of Stephenson Bastion. Sample SB1/J29 is from a glacially smoothed slab, complete with striations on a surface with patches of till, a partly clay matrix and striated clasts. Sample SB2/J31 comes from a weathered quartzite surface with many loose blocks (Fogwill *et al.*, 2004). Four samples (NL1/J22, CF157-08, CF158-08, CF162-08) come from gneiss bedrock on the slopes of the convex, ice-moulded summit of Mount Provender (950 m), while another sample (CF159-08) is from a gneiss erratic block on the same hill. These latter four samples from Mt. Provender were collected during a more recent expedition in 2008.

The sampling density over a large mountain area leaves much to be desired; it reflects both the inaccessibility of the Shackleton Range and the fact that one of the authors broke his leg in the field and had to be evacuated! Nonetheless, even sparse evidence from such a remote area is valuable. Since the samples were collected by different expeditions on different occasions and have been analysed for different isotopes in different laboratories over a succession of years, we bring together all the results in Tables 1 and 2 in standardised form. Also for coherence we describe the analytical methods in detail.

Whole rock samples were crushed and sieved to obtain the 250-710 µm fraction. The ^{10}Be and ^{26}Al isotopes were selectively extracted from the quartz component of the whole-rock sample at the University of Edinburgh's Cosmogenic Nuclide Laboratory following procedures adapted from the methods of Bierman *et al.* (2002) and Kohl and Nishiizumi (1992). Measurements of ^{10}Be/^{9}Be and ^{26}Al/^{27}Al isotopic ratios made in 2011 were conducted at the AMS facility at the Scottish Universities Environmental Research Centre (SUERC) in Glasgow, UK (Table 1). Measurements are normalised to the NIST SRM-4325 Be standard material with a revised (Nishiizumi *et al.*, 2007) nominal ^{10}Be/^{9}Be ratio of 2.79×10^{-11} and half-life of 1.387 Ma (Chmeleff *et al.*, 2010; Korschinek *et al.*, 2010), and the Purdue Z92-0222 Al standard material with a nominal ^{26}Al/^{27}Al ratio of 4.11×10^{-11} which agrees with the Al standard material of Nishiizumi (2004) with half-life of 0.705 Ma (Xu *et al.*, 2010). ^{10}Be/^{9}Be and ^{26}Al/^{27}Al isotopic ratios measured in 2006 at the ETH tandem AMS facility in Zurich, Switzerland, were normalised to their in-house S555 Be standard material and the ZAL94 Al standard material; the data in Table 1 have been renormalized (Kubik and Christl, 2010, Christl *et al.*, 2013) to be consistent with the SUERC data and therefore the 07KNSTD (Be) and KNSTD (Al) standards (Nishiizumi *et al.*, 2007; Nishiizumi, 2004).

Neon isotopes were measured in ~250 mg of quartz (250-500µm). Samples were wrapped in aluminium foil and loaded into a Monax glass tree and evacuated to $<10^{-8}$ torr for 48 hours prior to analysis. Samples were successively heated for 20 minutes to 1200°C in a double vacuum resistance furnace with a tungsten heating element and a molybdenum crucible. The extracted gas was cleaned on two hot SAES TiZr getters. The heavy noble gases (Ar, Kr and Xe) were successively absorbed onto two charcoal traps cooled with liquid nitrogen. Neon was then absorbed on to a charcoal trap at -228°C for 20 minutes and the residual He removed by a turbo-molecular pump. The Ne was released from the charcoal at -173°C and the isotopic composition analysed using a MAP 215-50 noble gas mass spectrometer fitted with a modified Nier-type ion source, an axial electron multiplier operated in pulse counting mode. Neon abundances were determined by peak height comparison with Ne from 95.2 ± 0.5 µcc

STP air. The reproducibility of noble gas abundances was better than ±1.5% and isotopic ratios of replicate calibrations were better than 0.5%. Interference corrections and detailed analytical procedure is presented elsewhere (Codillean *et al.*, 2008). Blanks at 1200°C were ^{20}Ne 1 x 10^{-11} ccSTP and were indistinguishable from the atmospheric isotopic composition.

For exposure age calculations we used default settings in Version 2.1 of the CosmoCalc programme (Vermeesch, 2007). Average production rates are 4.3 atoms $g^{-1}a^{-1}$ for ^{10}Be, 30.95 atoms $g^{-1}a^{-1}$ for ^{26}Al and 18.18 atoms $g^{-1}a^{-1}$ a for ^{21}Ne at sea-level, high-latitude scaled according to Stone (2000). The ^{21}Ne production rate is tied to the ^{10}Be production rate with a ^{21}Ne/^{10}Be ratio of 4.23 (Kober *et al.*, 2011). Local production rates reflect lower atmospheric pressure over Antarctica (Stone, 2000). No corrections are made for rock surface erosion or snow cover and thus exposure ages are minima.

4. Results

Table 1 lists sample details and nuclide concentrations, while Table 2 lists the calculated exposure ages. The relationship between ^{26}Al and ^{10}Be is shown graphically in an erosion island diagram which plots the ^{26}Al/^{10}Be ratios against the ^{10}Be concentration (Fig. 4a). Since the half lives of the two nuclides differ, this approach helps identify significant periods of burial, for example by ice. All samples lie outside of the erosion island including one anomaly with a high ^{26}Al/^{10}Be ratio (CF157). At face value most ratios indicate burial of 200 – 300 ka, assuming no rock surface erosion, while one sample from the Read Mountains (AC2/F2), a quartz vein, could indicate burial of c. 500 ka. However, the uncertainties are of a similar magnitude and this means that continuous exposure cannot be excluded. The ^{10}Be exposure ages come mostly from bedrock surfaces and those at higher altitudes above 1300 m in the Read Mountains, Stephenson Bastion and Lister Heights range from 1.4-2.5 Ma, indicating exposure for at least this length of time. Thus, if one excludes the anomaly with a high ^{26}Al/^{10}Be ratio (CF157), the new ^{26}Al and ^{10}Be data from a wider range of sites agree with the pilot study in suggesting that the mountains have been largely ice free for at least the last 1.5- 2.5 Ma. Further, the complex exposures could imply that they may have been buried by ice for an additional few hundred thousand years, either by the main ice sheet or a local ice cap.

Two ^{10}Be exposure ages at altitudes below 900 m on Mt. Provender have a lower age range of 0.6-0.7 Ma. Since the samples also lie outside the erosion island (but overlap within uncertainties), the values indicate that both bedrock and a glacial erratic on Mount Provender have been ice free for this length of time, perhaps with an additional period of burial. A third sample from Mount Provender (CF 162) displays a complex history, indicating a longer period of burial.

The cosmogenic ^{21}Ne concentrations of samples from above 1600 m are consistent with exposure for 1.8-2.5 Ma and are essentially similar to the ^{10}Be ages. Comparison of ^{21}Ne and ^{10}Be concentrations reveals that most samples have had continuous exposure for the last few million years, since they fall within the erosion island (Fig. 4b). Interestingly, the two samples from the lower slopes of Mount Provender (CF158 and CF157) lie outside the erosion island and indicate a complex exposure history amounting to several hundred thousand years of burial.

It is interesting to note that the ratios involving ^{26}Al with ^{10}Be and ^{21}Ne are inconsistent in a few samples. For example, $^{26}Al/^{10}Be$ ratios for samples CF162 and AC2/F2 imply considerable burial of c. 500 ka while the $^{21}Ne/^{10}Be$ ratios do not. Likewise, the $^{26}Al/^{10}Be$ ratio for sample CF157 was erroneously high while, in contrast, the $^{21}Ne/^{10}Be$ ratio suggests burial. Given the overall consistency in the ^{21}Ne and ^{10}Be concentrations, it seems probable that the discrepancies reflect errors in the recovery of ^{26}Al. Thus in the discussion we rely more heavily on the ^{21}Ne and ^{10}Be results.

5. Discussion

The ^{26}Al, ^{10}Be and ^{21}Ne concentrations from a wider range of summit sites agree with the pilot study (Fogwill *et al.* 2004) and suggest that the high glaciated surfaces have remained largely ice-free for at least the last 1.5- 2.5 Ma. This implies that the glacial overriding of at least the higher summits of the Shackleton Range took place earlier than ~2.5 million years ago. Since the exposure ages do not take into account the erosion of the rock surfaces or potential removal of overlying till, these are minimum ages. The younger values at lower altitude, with evidence of complex exposure histories in two bedrock samples, may indicate a further period of significant ice cover on the lower slopes of the northwest Shackleton Range.

When might the troughs of the Slessor and Recovery glaciers have been cut? By drawing inferences from elsewhere in Antarctica, one possibility is that they formed around 14 Ma in the mid-Miocene or earlier. This would be similar to the Dry Valleys and the Lambert Glacier areas where overriding ice eroded troughs. In the case of the Dry Valleys, mid-Miocene marine deposits exist on the floors of the glaciated Wright and Taylor valleys, demonstrating that the troughs had been deepened by the mid-Miocene (Hall *et al.,* 1993; Webb and Wrenn, 1982). Moreover, the troughs have not been occupied by overriding ice in the last 14 Ma. On the basis of deposits in Prydz Bay, the Lambert trough is also argued to have been excavated by ice extending to the continental shelf by the mid-Miocene. Since then a change in offshore sediments and modelling imply that the outlet glacier has been confined to the trough for the last ~14 Ma (Taylor *et al.,* 2004).

Perhaps the overdeepened troughs on either side of the Shackleton Range and offshore represent a comparable situation. There are several reasons for believing that most erosion would have occurred early in the glaciation of Antarctica. First, it is likely that the cyclic glacial episodes from ~34 Ma to ~17 Ma recognised in the till/meltwater couplets in the Cape Roberts' sediment cores, occurred during warmer than present climates (Naish *et al.,* 2001). Such early ice sheets are modelled to be widely associated with subglacial meltwater which would have aided erosion (Jamieson *et al.* 2010). Secondly, these early ice sheets are thought to have extended to the edge of the continental shelf surrounding Antarctica, while, at least in East Antarctica, ice has been restricted to the continent over the last 13.6 Ma (Anderson, 1999). It makes sense to regard the Slessor and Recovery troughs, flowing into the Thiel/Filchner trough, as part of this larger continental flow, as argued elsewhere (Hein *et al.,* 2011). Thirdly, there are theoretical grounds for believing that an ice sheet created on a fluvial landscape would quickly carve a bed better adjusted to the discharge of ice (Kessler *et al.,* 2008; Jamieson *et al.,* 2008). Troughs facilitate the discharge of ice through bounding mountains and are likely to be created early in a glacial episode. Could the excavation of the troughs by such early ice sheets be

responsible for the lowering of the ice surface and the rerouting of ice flow around the Shackleton Range?

Perspective on the processes involved can be gained by simple calculations. We can assume that the pre-glacial coast lay immediately off the Shackleton block and that the river valleys bounding the mountains to the north and south were graded to sea level. In the absence of troughs, and taking a simple model assuming perfect plastic behaviour and a horizontal base, an ice sheet would build up with ice-surface gradients approximating to a parabola rising inland from the coast and reaching elevations of 1000 m at 50 km and 1500 m at 100 km (Nye, 1952). This compares with the present ice surface slope along the Slessor Glacier with elevations rising from 100 m near the grounding line to 250 m at 50 km and 500 m at 100 km inland. Even allowing for the simplicity of the assumptions, the transformation of a pre-existing river valley into a trough suitable for outlet-glacier flow reduces ice surface elevations in the vicinity of the Shackleton Range by an order of 750-1000 m.

The isostatic effect of removing the mass of rock to form the glacial troughs can also be approximated. The massif is 80 km across and bounded by the 50 km-wide Slessor and 70 km-wide Recovery valleys, both assumed to be close to sea level before glaciation. Figure 5 shows a cross section across the troughs at a point ~150 km from the edge of the mountain block. The upper panel shows the initial state of glaciation with an ice sheet surface altitude of ~2000 m submerging the mountains. The ice surface slopes from south to north to represent the evidence of flow across the mountains. No adjustment is made for isostatic depression under the ice load. Figure 5 (lower panel) shows the ice surface and bed topography today, the latter reflecting the deepening caused by glacial erosion. The cross-sectional area of glacially eroded rock is 58 km^2 and 108 km^2 in the case of the Slessor and Recovery troughs respectively. We assume a constant depth of ice during excavation, although its distribution changes, and also that the crust remains rigid over such a relatively short distance. Allowing for removal of rock from the cross-sectional areas of these valleys would cause isostatic uplift of the area, including the intervening Shackleton Range, by approximately 800 m. It is important to stress that this is a value obtained for a cross section of the mountains where the troughs are deepest. In reality the overdeepened basins are restricted spatially and thus if erosion is averaged over a wider area, the isostatic compensation will be less.

The implication of these simple calculations is sufficient to demonstrate the viability of a process whereby glacial erosion of outlet glacier troughs lowers the adjacent ice sheet surface and exposes adjacent mountain massifs. In the case of the Shackleton Range, field observations show that the deepening of the surrounding troughs lowered the ice-sheet surface relative to the mountains by a minimum of 650 m, which is the height of the bounding trough walls overlooking Recovery Glacier. Since the ice flowed across the massif, the relative lowering must have been more, perhaps by several hundred metres, giving a total lowering relative to the mountains at least of the order of 800-1000 m.

Our data indicate that the lowering occurred earlier than 2.5 Ma and, by analogy with elsewhere in Antarctica, it is likely that much of this had been achieved by the mid Miocene. It is possible that the younger dates on Mt Provender represent an intermediate stage of relative lowering, perhaps within the last few million years. If

so, this may have been the ice sheet that deposited erratics with ^{21}Ne exposure ages of 0.8 Ma years on the mountain slopes. Alternatively, this phase could be related to changes in ice thickness linked to early Quaternary climatic cycles. Subsequent relative lowering of ~150 m during the Quaternary has been suggested on the basis of the interpretation of exposure ages of glacial deposits on the flanks of the Slessor Glacier (Hein *et al.*, 2013)

The role of the processes involved in the excavation of troughs and their effect on lowering relative ice surface elevations are coupled and difficult to disentangle. The transformation of a fluvial valley, perhaps with interlocking spurs, into a trough form to permit low-gradient ice-stream flow does not necessarily involve rock uplift and yet it will lower ice surface elevations. But rock uplift by isostatic compensation makes the excavation of a deep trough easier to envisage. Moreover it introduces a feedback mechanism whereby ice is increasingly channelled down the troughs and around any intervening mountains, thus increasing the potential for further deepening of the troughs. Such a process is suggested by the coincidence of the overdeepened basins with ice flow which is progressively confined as it circumvents the mountain massif (Fig. 2).

One can speculate further on the macro-geomorphology of the Shackleton Range. Perhaps its morphology and lack of Beacon Supergroup cover rocks is due to the chance that two major continental river valleys discharged from the continent only 80 km apart. Excessive deepening of troughs on either side may have caused an unusually high amount of uplift. In such a case the uplift may have been of basement rocks originally exposed as a result of base-level lowering at the coast following continental break up. Such a coastal erosion surface cut in basement rocks occurs in the Transantarctic Mountains in the McMurdo Dry Valleys and is typical of passive continental margins (Kerr *et al.*, 2000). Even further, could the tilt of the Shackleton block with the highest elevations along the southern flank of the massif be due to differential rock uplift because of the contrast between the volumes of the two bounding troughs? In other words excavation of the larger Recovery trough has caused more flank uplift than the smaller Slessor trough.

It could be argued that tectonic uplift of the massif could equally well explain the emergence of the Shackleton Mountains above the ice-sheet surface. The role of such movements cannot be ruled out, but the presence of gentle fluvial slopes associated with river valleys flowing towards the Slessor valley at an elevation of only 240 m would seem to rule out significant tectonic uplift, at least since initial glaciation.

6. Conclusion

This paper studies a subglacial fjord landscape in the Shackleton Range, Antarctica and presents evidence that ice-sheet erosion of troughs across a passive continental margin caused the adjacent mountains to emerge above the ice-sheet surface. Use of multiple cosmogenic isotopes help establish that the overriding and deepening of the troughs occurred earlier than the Quaternary. We suggest significant erosion occurred in the mid Miocene maximum, as elsewhere in East Antarctica in the Dry Valleys and the Lambert trough.

The main implication of the paper is that the erosional processes which deepen the bed of an ice sheet increase the topographic relief and can change the thickness, extent

and direction of overriding ice flow. Our dating in Antarctica is too limited to establish the rates of landscape evolution by ice sheets. Nevertheless, it reveals that excavation of troughs over millions of years caused the Shackleton Range to be exposed and this changed the flow of the surrounding ice sheet.

Acknowledgements

We acknowledge the financial support of the UK Natural Environment Research Council (NERC), Australian Research Council (ARC) and Antarctic Logistics and Expeditions (ALE) for much of the logistic support. We thank Johan Kleman and two anonymous referees for valuable comments on the paper.

References

Altmaier, M., Herpers, U., Delisle, G., Merchel, S., Ott, U., 2010. Glaciation history of Queen Maud Land (Antarctica) reconstructed from in-situ produced cosmogenic ^{10}Be, ^{26}Al and ^{21}Ne. Polar Science, 4, 42-61.

Anderson, J.B., 1999. Antarctic marine geology. Cambridge University Press, Cambridge, 289 pp.

Augustinus, P.C., 1992. The influence of rock mass strength on glacial valley cross-profile morphometry: a case study from the Southern Alps, New Zealand. Earth Surface Processes and Landforms, 17, 39-51.

Bamber, J.L., Ferraccioli, F., Joughin, I., Shepherd, T., Rippin, D.M., Siegert, M.J., Vaughan, D.G., 2006. East Antarctic ice stream tributary underlain by major sedimentary basin. Geology, 34, 33-36.

Beaumont, C., Looi, H., Willet, S. 2000. Coupled tectonic-surface process models with applications to rifted margins and collisional orogens. In: Summerfield, M.A. (Ed.), Geomorphology and global tectonics. Wiley, 29-55.

Bierman, P.R., Caffee, M.W., Davis, P.T., Marsella, K., Pavich, M., Colgan, P., Mickelson, D., Larsen, J., 2002. Rates and timing of earth surface processes from in situ-produced cosmogenic Be-10, Beryllium: Mineralogy, Petrology and Geochemistry. Volume 50: Reviews in Mineralogy & Geochemistry: Washington, Mineralogical Soc America, 147-205.

Bo, S., Siegert, M.J., Mudd, S.M., Sugden, D.E., Fujita, S., Xiangbin, C., Yunyun, J., Xueyuan, T., Yuansheng, L. 2009. The Gamburtsev mountains and the origin and early evolution of the Antarctic Ice Sheet. Nature, 459,690-693 (doi:10.1038/nature08024)

Bretz, J.H. 1935. Physiographic studies in East Greenland. In Boyd, L.A., (ed.), The fiord region of East Greenland. Amer. Geogr. Soc. Spec. Pub. 18, 161-266.

Briner, J.P., Miller, G.H.,, Finkel, R., Hess, D.P., 2008. Glacial erosion at the fjord onset zone and implications for the organization of ice flow on Baffin Island, Arctic Canada. Geomorphology, 97, 126-134.

Chmeleff, J., von Blanckenburg, F., Kossert, K., and Jakob, D., 2010, Determination of the Be-10 half-life by multicollector ICP-MS and liquid scintillation counting: Nuclear Instruments & Methods in Physics Research Section B, Beam Interactions with Materials and Atoms, 268, 192-199.

Christl, M., Vockenhuber, C., Kubik, P.W., Wacker, L., Lachner, J., Alfimov, V., Synal, H.-A., 2013. The ETH Zurich AMS facilities: performance parameters and reference materials. Nuclear Instruments and Methods in Physics Research B, 294, 29-38

Codilean, A.T., Bishop, P., Stuart, F.M., Hoey, T.B., Fabel, D., Freeman, S.P.H.T., 2008. Single-grain cosmogenic ^{21}Ne concentrations in fluvial sediments reveal spatially variable erosion rates. Geology 36, 159-162.

Di Nicola, L., Strasky, S., Schlüchter, C., Salvatore, M.C., Akçar, N., Kubik, P.W., Christl, M., Kasper, H.U., Wieler, R., Baroni, C., 2009. Multiple cosmogenic nuclides document complex Pleistocene exposure history of glacial drifts in Terra Nova Bay (northern Victoria Land, Antarctica). Quaternary Research, 71, 83-92.

Dunai,T.J. 2000. Scaling factors for production rates of in situ-produced cosmogenic nuclides: a critical re-evaluation. Earth Planet. Sci. Lett., 176, 157-169.

Fitzgerald, P.G., 1992. The Transantarctic Mountains of southern Victoria Land: the application of apatite fission track analysis to a rift shoulder uplift. Tectonics, 11, 634-662.

Fogwill, C.J., Bentley, M.J., Sugden, D.E., Kerr, A.R., Kubik, P., 2004. Cosmogenic nuclides ^{10}Be and ^{26}Al imply limited Antarctic ice sheet thickening and low erosion in the Shackleton range for > 1 m.y. Geology, 32, 265-268.

Fretwell, P. and 59 others, 2013. Bedmap 2: improved ice bed, surface and thickness datasets for Antarctica. The Cryosphere, 7, 375-393.

Hall, B.L., Denton, G.H., Lux, D.R., Bockheim, J.G., 1993. Late Tertiary Antarctic paleoclimate and ice-sheet dynamics inferred from surficial deposits in Wright Valley. Geogr. Annlr., 75A, 239-267.
Hambrey, M.J., Glasser, N.F., McKelvey, B.C., Sugden, D.E., Fink, D. 2007. Cenozoic landscape evolution of an East Antarctic oasis (Radok Lake area, northern Prince Charles Mountains, and its implications for the glacial and climatic history of Antarctica. Quat. Sci.Rev., 26, 598-626.
Hein, A.S., Fogwill, C.J., Sugden, D.E., Xu, S., 2011. Glacial/interglacial ice-steam stability in the Weddell Sea embayment, Antarctica. Earth & Planet. Sci. Lett., 307, 211-221.
Hein, A.S., Fogwill, C.J., Sugden, D.E., Xu, S., 2013. Interpreting the scatter of cosmogenic-nuclide exposure ages in the Shackleton Range, Antarctica: implications for glacial history. Quaternary Chronology, In press
Holtedahl, H., 1967. Notes on the formation of fjords and fjord valleys. Geogr. Annlr., 49A, 188-203.
Høfle, H-C., 1980. Glazialgeologische Untersuchungen im Transantarktischen Gebirge (Ost-Antarktis). Westfälische Geogr. Stud. 36, 41-52.
Höfle, H.C., Buggisch, W., 1995. Glacial geology and petrography of erratics in the Shackleton Range, Antarctica. Polarforschung, 63, 183-201.
Jamieson, S.S.R., Hulton, N.R.J., Hagdorn, M., 2008. Modelling landscape evolution under ice sheets. Geomorphology, 97, 91-108.
Jamieson, S.S.R., Sugden, D.E., Hulton, N.R.J., 2010. The evolution of the subglacial landscape of Antarctica. Earth & Planet. Sci Lett., 293, 1-27.
Jamieson, S.S.R., Sugden, D.E., 2008. Landscape evolution of Antarctica. In: Cooper, A. and editorial team, (Eds.), Antarctica a keystone in a changing world. National Academies Press, 39-54.
Joughin, I. and Bamber, J.L., 2005. Thickening of the ice stream catchments feeding the Filchner-Ronne Ice Shelf, Antarctica. Geophys. Res. Lett., 32, 4.
Joughin, I., Bamber, J.L., Scambos, T., Tulaczyk, S., Fahnestock, M., Macayeal, D.R., 2006. Integrating satellite observations with modelling: basal shear stress of the Filchner-Ronne ice streams, Antarctica. Phil. Trans. Roy. Soc., 364, 1795-1814.
Kerr, A.R., Gilchrist, A.R., 1996. Glaciation, erosion and the evolution of the Transantarctic Mountains, Antarctica. Ann. Glaciol., 23, 303-308.
Kerr, A., Hermichen, W.D., 1999. Glacial modification of the Shackleton Range, Antarctica. Terra Antartica., 6, 353-360.
Kerr, A., Sugden, D.E., Summerfield, M.A., 2000. Linking tectonics and landscape development in a passive margin setting: the Transantarctic Mountains. In: Summerfield, M.A. (ed) Geomorphology and global tectonics. Wiley, 303-319.
Kessler, M.A., Andersen, R.S., Briner, J.P., 2008. Fjord insertion into continental margins driven by topographic steering of ice. *Nature Geosc.*, doi:10.1038/ngeo201:1-5
Kleman, J., Stroeven, A.P., Lundqvist, J., 2008. Patterns of Quaternary ice sheet erosion and deposition in Fennoscandia and a theoretical framework for explanation. Geomorphology, 97, 73-90.
Løken, O.H. and Hodgson, D.A. 1971. On the submarine geomorphology along the east coast of Baffin Island. Can. J. Earth Sci. 8, 185-195.
Kober, F., Alfimov, V., Ivy-Ochs, S., Kubik, P.W., and Wieler, R., 2011, The cosmogenic (NE)-N-21 production rate in quartz evaluated on a large set of existing Ne-21-Be-10 data: *Earth Plan. Sci.Lett.*, 302, 163-171.
Kohl, C.P., and Nishiizumi, K., 1992, Chemical Isolation of Quartz for Measurement of in situ-Produced Cosmogenic Nuclides: *Geochimica et Cosmochimica Acta*, 56, 3583-3587.
Korschinek, G., Bergmaier, A., Faestermann, T., Gerstmann, U.C., Knie, K., Rugel, G., Wallner, A., Dillmann, I., Dollinger, G., von Gostomski, C.L., Kossert, K., Maiti, M., Poutivtsev, M., and Remmert, A., 2010. A new value for the half-life of Be-10 by Heavy-Ion Elastic Recoil Detection and liquid scintillation counting: Nuclear Instruments & Methods in Physics Research Section B, Beam Interactions with Materials and Atoms, 268, 187-191.
Kubik, P.W., and Christl, M., 2010, Be-10 and Al-26 measurements at the Zurich 6 MV Tandem AMS facility. Nuclear Instruments & Methods in Physics Research Section B, Beam Interactions with Materials and Atoms, 268, 880-883.
Makinson,K., Nicholls, K.W., 2011. Modeling tidal currents beneath Filchner-Ronne Ice Shelf: their effect on mixing and transport. J. Geophys. Res. Oceans, 104, 13449-13465.
Marchant, D.R., Swisher III, C.C., Lux, D.R., West Jr, D.P., Denton, G.H. 1993. Pliocene paleoclimate and East Antarctic ice-sheet history from surficial ash deposits. Science, 260, 667-670.
Naish, T.R., and 32 others, 2001. Orbitally induced oscillations in the East Antarctic Ice Sheet at the Oligocene/Miocene boundary, Nature, 413, 719-723.
Nishiizumi, K., 2004. Preparation of Al-26 AMS standards. Nuclear Instruments & Methods in Physics Research Section B, 223-24, 388-392.

Nishiizumi, K., Imamura, M., Caffee, M.W., Southon, J.R., Finkel, R.C., and McAninch, J., 2007. Absolute calibration of Be-10 AMS standards: Nuclear Instruments & Methods in Physics Research Section B, 258, 403-413.
Nye, J.F., 1952. A method of calculating the thickness of ice sheets, Nature, 169 (4300), 529-530.
Rippin, D.M., Siegert, M.J., Bamber, J.L., Vaughan, D.G., Corr, H.F.J., 2006. Switch-off of a major enhanced ice flow unit in East Antarctica. Geophys. Res. Lett., 33, doi:10.1029/2006GL026648.
Rogenhagen,J., Jokat, W., Hinz, K., Kristofferson, Y., 2004. Improved seismic stratigraphy of the Mesozoic Weddell Sea. Mar. Geophys. Res., 25, 265-282.
Rose, K.C., Ferraccioli, F., Jamieson, S.S.R., Bell, R.E., Corr, H., Creyts, T.T., Braaten, D., Jordan, T.A., Fretwell, P.T., Damaske, D., 2013. Early East Antarctic Ice Sheet growth recorded in the landscape of the Gamburtsev Subglacial Mountains. Earth & Planet. Sci. Lett., http://dx.doi.org/10.1016/jepsl.2013.03.053.
Skidmore, M.J., Clarkson, P.D., 1972. Physiography and glacial geomorphology of the Shackleton Range. Brit. Ant. Surv. Bull., 30, 69-80.
Stephenson, P.J. 1966. Geology 1. Theron Mountains, Shackleton Range and Whichaway Nunataks. Scientific Reports of the Transantarctic Expedition, London, 8, 79pp
Stern, T.A., Baxter, A.K., Barrett, P.J., 2005. Isostatic rebound due to glacial erosion within the Transantarctic Mountains. Geology, 33, 221-224
Stone, J.O., 2000. Air pressure and cosmogenic isotope production. J. Geophys. Res. Solid Earth, 105, 23,753-23,759.
Stone,J.O., Balco, G.A., Sugden, D.E., Caffee, M.W., Sass, L.C., Cowdery, S.G., Siddoway, C., 2003 Holocene deglaciation of Marie Byrd Land, West Antarctica. Science, 299, 99-102.
Sugden, D.E. and Denton, G.H. 2004. Cenozoic landscape evolution of the Convoy Range to Mackay Glacier area: onshore to offshore synthesis. Bull. Geol. Soc. Amer. 116, 840-857.
Sugden, D.E. and John, B.S. 1976. *Glaciers and Landscape* Arnold, p. 206 (Fig10.12)
Sugden, D.E., Balco, G., Cowdery, S.G., Stone, J.O.,Sass, L.C., 2005. Selective glacial erosion and weathering zones in the coastal mountains of Marie Byrd Land, Antarctica. Geomorphology, 67, 317-334.
Swift, D.A., Persano,C., Stuart, F.M., Gallagher, K., Whitham, A., 2008. A reassessment of the role of ice sheet glaciation in the long-term evolution of the East Greenland Fjord region. Geomorphology, 97, 109-125.
Taylor, J., Siegert, M.J., Payne, A.J., Hambrey, M.J., O'Brien, P.E., Cooper, A.K., Leitchenkov, G., 2004. Topographic controls on post-Oligocene changes in ice-sheet dynamics, Prydz Bay region, East Antarctica. Geology, 32, 197-200.
Thomson, S.N., Reiners, P.W., Hemming, S.R., Gehrels, G.E., 2013. The contribution of glacial erosion to shaping the hidden landscape of East Antarctica. Nature Geosc., 6, 203-207.
Vermeesch, P, 2007. CosmoCalc: An Excel add-in for cosmogenic nuclide calculations, Geochemistry Geophysics Geosystems, V.8, 8, 1-14.
Tomkin, J.H., 2003. Erosional feedbacks and the oscillations of ice masses. J. Geophys. Res., 108 (B10), 2488, doi:10.1029/2002JB002087
Webb, P-N., 1994. Paleo-drainage systems of East Antarctica and sediment supply to West Antarctic Rift System basins. Terra Antartica, 1, 457-461.
Webb, P-N., Wrenn, J., 1982. Upper Cenozoic biostratigraphy and micropaleontology of Taylor Valley, Antarctica. In: Craddock, C. (ed.) Antarctic Geoscience, University of Wisconsin Press, Madison, 117-122.
Xu, S., Dougans, A.B., Freeman, S., Schnabel, C., and Wilcken, K.M., 2010, Improved Be-10 and Al-26-AMS with a 5 MV spectrometer. Nuclear Instruments & Methods in Physics Research Section B, Beam Interactions with Materials and Atoms, 268, 736-738.

List of Figures

Figure 1. The Shackleton Range in Antarctica, situated between the Slessor and Recovery outlet glaciers of the East Antarctic Ice Sheet, overlooks the Filchner Ice Shelf which floats above the deep submarine Thiel trough. Map shows the location of the geomorphology map in Figure 3 and the Read Mountains. The red colours indicate fast ice flow up to 1500 m/yr. After Joughin and Bamber (2005)

Figure 2. The topography of the Shackleton Range and its bounding Slessor and Recovery outlet glacier troughs, showing remarkable overdeepening on either side of the mountain block and the deep Thiel trough to the west. The transverse black line A-B is the location of the cross section of the glacier and subglacial bed topography in Figure 5. After Fretwell *et al.,* (2013).

Figure 3. Geomorphological map of the landforms of the western Shackleton Range showing, surfaces, escarpments, rectilinear slopes and inselbergs. The arrows indicate the direction of flow of overriding ice. The Read Mountains lie to the east of the mapped area. Compiled from air photographs flown in 1986 by the Institute for Applied Geodesy, Frankfurt, Germany. The upper photograph is of the inselberg landscape with rectilinear slopes adjacent to Slessor Glacier. The lower photograph shows the location of sample site SB1/J29 on the plateau edge at Stephenson Bastion. The site overlooks Recovery Glacier hundreds of metres below.

Figure 4. (a) Erosion island diagram of the radionuclide $^{26}Al/^{10}Be$, plotted against the concentration of ^{10}Be. The ellipses represent the total 1-sigma errors for the samples. The dark lines represent the erosion island, indicating a simple exposure history. The lines projecting down from this relate to erosion, and the lower curves represent the modelled effects of burial on the ratios. There is an overlapping older cluster of samples (AC, SB, LH) from the higher-elevation Read Mountains, Stephenson Bastion and Lister Heights and a younger cluster (CF) from Mount Provender. (b) Erosion island diagram showing the relationship between $^{21}Ne/^{10}Be$ and ^{10}Be concentration. The lines projecting upwards relate to erosion rates and the upper curves model the effect of burial. Plots created using CosmoCalc Version 2.1 (Vermeesch, 2007).

Figure 5. Upper panel. At the onset of ice-sheet glaciation this cross section, transverse to modern ice flow, shows the mountains bounded by the Slessor and Recovery valleys graded to contemporary sea level. The idealised ice surface profile after Nye (1952) assumes a horizontal bed and is shown for a distance 150 km from the edge of the Thiel trough, but with an additional gradient from south to north to reflect the flow of overriding ice. No adjustment is made for glacio-isostatic depression beneath the ice load.
Lower panel. The situation today showing the present ice surface and glacier bed. Isostatic recovery has uplifted the mountain block in response to the loss of a mass of rock eroded by deep troughs cut into the Slessor and Recovery river valleys. For simplicity we assume the ice load is the same in both scenarios. Bed and ice surface topography after Fretwell *et al.,* 2013).

Table 1: Sample details and cosmogenic nuclide data, Shackleton Range, Antarctica.

Table 2: Exposure ages and ratios, Shackleton Range, Antarctica.

Table 1

Table 1. Cosmogenic nuclide data

#	Sample ID	Year[a]	Repeats[a]	Lat (dd)	Long (dd)	Alt (m)	Thick (cm)	Density (g/cm^3)	Topo scaling factor	^{10}Be conc[b] (at/g SiO_2)	^{10}Be ± 1σ	^{26}Al conc[b] (at/g SiO_2)	^{26}Al ± 1σ	^{21}Ne conc (at/g SiO_2)	^{21}Ne ± 1σ
Read Mountains															
1	AC2/F2	**2006**		-80.65	-23.97	1890	5	2.65	0.995	3.53E+07	2.26E+06	1.09E+08	8.37E+06	2.65E+08	1.60E+07
2	AC3/F3 (a)	**2006**		-80.66	-23.38	1890	5	2.65	0.995	3.41E+07	2.19E+06	1.27E+08	9.77E+06	2.95E+08	1.30E+07
	AC3/F3 (b)	**2011**	**^{21}Ne**	"	"	"	"	"	"	"	"	"	"	2.91E+08	9.08E+06
3	AC1/F2 (a)	**2006**		-80.65	-24.12	1680	5	2.65	0.995	3.31E+07	2.32E+06	1.23E+08	9.49E+06	2.14E+08	1.30E+07
	AC1/F2 (b)	**2006**	**^{10}Be**	"	"	"	"	"	"	3.18E+07	2.42E+06	"	"	"	"
Stephenson Bastion															
4	SB2/J31	**2006**		-80.77	-26.97	1785	5	2.65	0.995	3.37E+07	1.73E+06	1.27E+08	9.40E+06	n/a	n/a
5	SB1/J29 (a)	**2006**		-80.77	-27.05	1600	5	2.65	0.995	2.21E+07	1.24E+06	9.43E+07	7.14E+06	2.11E+08	1.00E+07
	SB1/J29 (b)	**2011**	**^{21}Ne**	"	"	"	"	"	"	"	"	"	"	1.72E+08	5.30E+06
Lister Heights															
6	LH1/J15 (a)	**2006**		-80.52	-28.54	1320	5	2.65	0.995	1.86E+07	1.09E+06	7.95E+07	6.20E+06	1.47E+08	6.80E+06
	LH1/J15 (b)	**2011**	**^{21}Ne**	"	"	"	"	"	"	"	"	"	"	1.44E+08	4.55E+06
	LH1/J15 (c)	**2011**	**^{21}Ne**	"	"	"	"	"	"	"	"	"	"	1.48E+08	4.83E+06
Mount Provender															
7	NL1/J22	**2006**		-80.37	-29.95	950	5	2.65	0.998	2.22E+07	1.22E+06	n/a	n/a	n/a	n/a
8	CF_162_08	**2011**		-80.38	-29.95	913	2.5	2.65	0.998	7.94E+06	1.78E+05	3.58E+07	1.83E+06	4.87E+07	1.58E+06
9	CF_159_08	**2011**		-80.38	-29.96	893	5	2.65	0.998	7.16E+06	1.60E+05	3.85E+07	1.96E+06	4.28E+07	1.43E+06
10	CF_158_08	**2011**		-80.38	-29.98	744	4.5	2.65	0.998	5.83E+06	1.31E+05	3.05E+07	1.56E+06	4.35E+07	1.36E+06
11	CF_157_08 (a	**2011**		-80.38	-30.00	600	4.5	2.65	0.998	6.16E+06	1.31E+05	4.42E+07	2.26E+06	6.12E+07	2.04E+06
	CF_157_08 (b	**2011**	**^{21}Ne**											5.83E+07	2.01E+06

[a] ^{10}Be and ^{26}Al samples prepared in 2006 were measured on the AMS at ETH Zurich; those prepared in 2011 and all ^{21}Ne measurements were made at the SUERC (see text).

[b] ^{26}Al and ^{10}Be concentrations have been renormalised to be consistent with the 07KNSTD Be standard (Nishiizumi et al., 2007) and the KNSDT Al standard (Nishiizumi, 2004).

^{26}Al and ^{10}Be process blanks were spiked with 250 µg ^{9}Be carrier (Scharlau Be carrier, 1000 mg/l, density 1.02 g/ml) and 1.5 mg ^{27}Al carrier (Fischer Al carrier, 1000 ppm).

Samples were spiked with 250 µg ^{9}Be carrier and up to 1.5 mg ^{27}Al carrier (the latter value varied depending on the native Al-content of the sample).

Concentrations of ^{26}Al and ^{10}Be are corrected for process blanks which contained <1% of the total ^{26}Al and ^{10}Be atoms in samples.

Uncertainties include propagated AMS sample/lab-blank uncertainty, 2% carrier mass uncertainty and 3% (2011) or 5% (2006) stable ^{27}Al measurement (ICP-OES) uncertainty.

Table 2

Table 2. Exposure ages

#	Sample ID	Year	Repeats	Alt (m)	^{10}Be age (Ma)	^{10}Be ± 1σ (Ma)	^{26}Al age (Ma)	^{26}Al ± 1σ (Ma)	^{21}Ne age (Ma)	^{21}Ne ± 1σ Ma)	^{26}Al/^{10}Be	^{21}Ne/^{10}Be	^{21}Ne/^{26}Al
Read Mountains													
1	AC2/F2	**2006**		1890	2.114	0.0836	0.824	0.0435	2.296	0.1388	3.09	7.51	2.43
2	AC3/F3 (a)	**2006**		1890	1.991	0.0808	1.063	0.0508	2.559	0.1128	3.73	8.66	2.32
	AC3/F3 (b)	**2011**	**^{21}Ne**		"	"	"	"	2.524	0.0788	"	8.54	2.29
3	AC1/F2 (a)	**2006**		1680	2.519	0.1003	1.355	0.0577	2.174	0.1320	3.73	6.47	1.73
	AC1/F2 (b)	**2006**	**^{10}Be**		2.338	0.1048	"	"	"	"	3.88	6.72	"
Stephenson Bastion													
4	SB2/J31	**2006**		1785	2.246	0.0691	1.231	0.0528	n/a	n/a	3.78	n/a	n/a
5	SB1/J29 (a)	**2006**		1600	1.419	0.0570	0.926	0.0461	2.280	0.1080	4.27	9.57	2.24
	SB1/J29 (b)	**2011**	**^{21}Ne**		"	"	"	"	1.858	0.0572	"	7.79	1.82
Lister Heights													
6	LH1/J15 (a)	**2006**		1320	1.540	0.0626	1.009	0.0500	1.986	0.0919	4.26	7.88	1.85
	LH1/J15 (b)	**2011**	**^{21}Ne**		"	"	"	"	1.941	0.0615	"	7.70	1.81
	LH1/J15 (c)	**2011**	**^{21}Ne**		"	"	"	"	1.999	0.0652	"	7.93	1.86
Mount Provender													
7	NL1/J22	**2006**		950	4.079	0.0959	n/a	n/a	n/a	n/a	n/a	n/a	n/a
8	CF_162_08	**2011**		913	0.759	0.0141	0.504	0.0203	0.908	0.0294	4.51	6.13	1.36
9	CF_159_08	**2011**		893	0.702	0.0132	0.582	0.0226	0.830	0.0277	5.37	5.98	1.11
10	CF_158_08	**2011**		744	0.641	0.0122	0.508	0.0205	0.961	0.0301	5.23	7.46	1.43
11	CF_157_08 (a)	**2011**		600	0.802	0.0140	1.067	0.0338	1.540	0.0514	7.18	9.93	1.38
	CF_157_08 (b)	**2011**	**^{21}Ne**		"	"	"	"	1.468	0.0507	"	9.47	1.32

Exposure ages calculated using Version 2.1 of the CosmoCalc programme (Vermeesch, 2008) using default settings.

Production rates are scaled according to Stone (2000) with lower 'Antarctic' air pressure conditions.

Exposure ages assume no rock surface erosion and uncertainties are analytical only.

Figure 1

Click here to download high resolution image

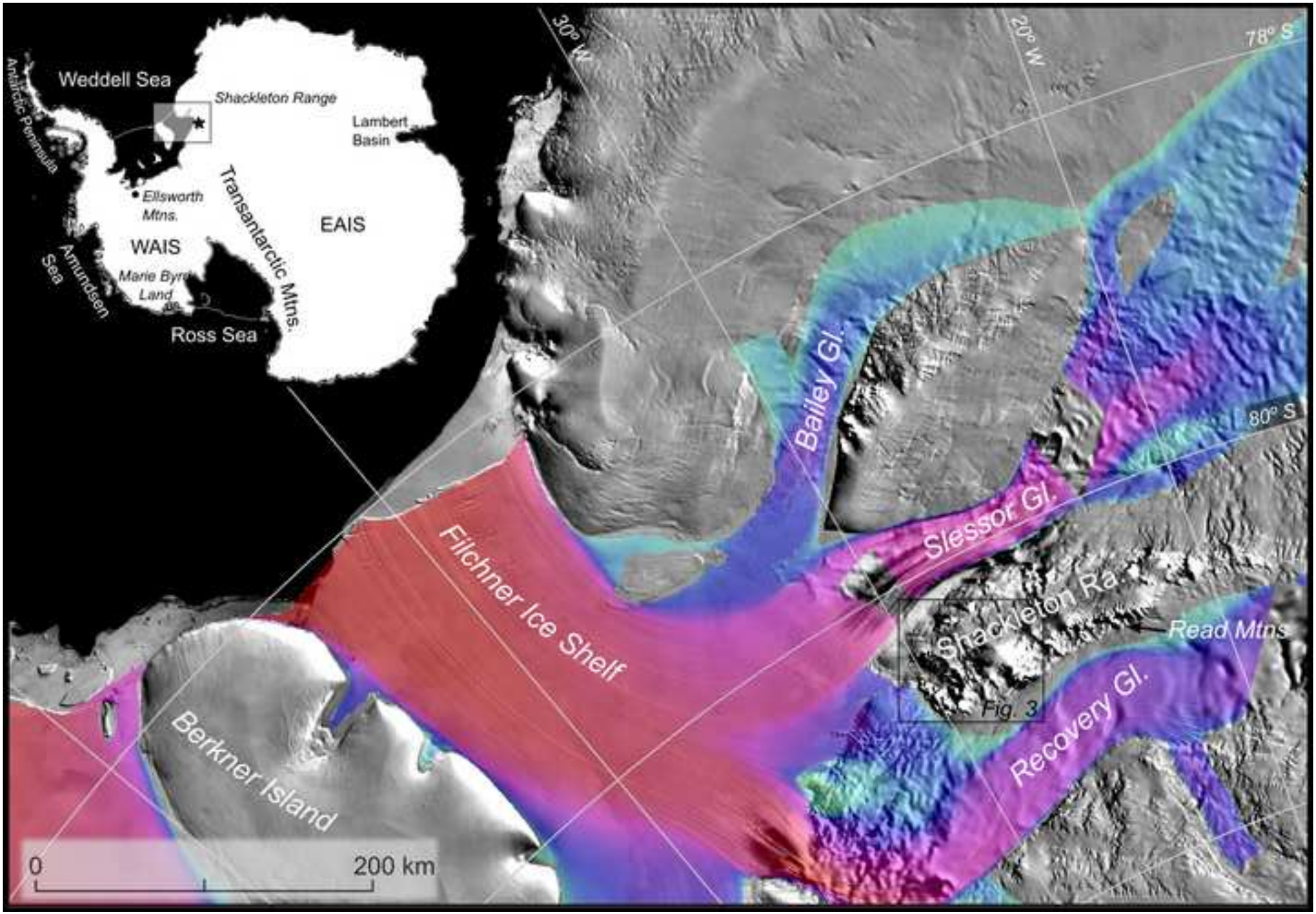

Figure 2

Click here to download high resolution image

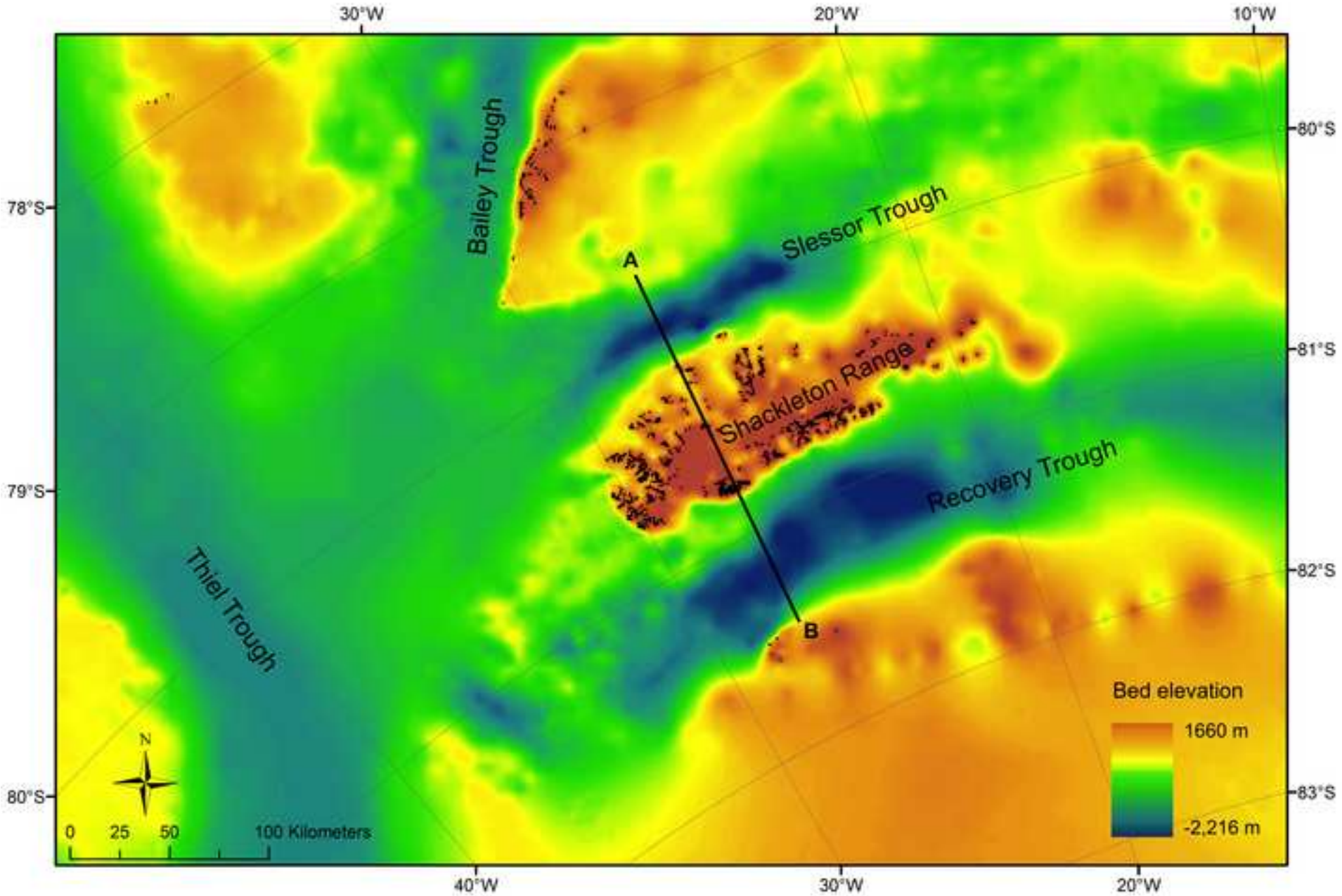

Figure 3

Click here to download high resolution image

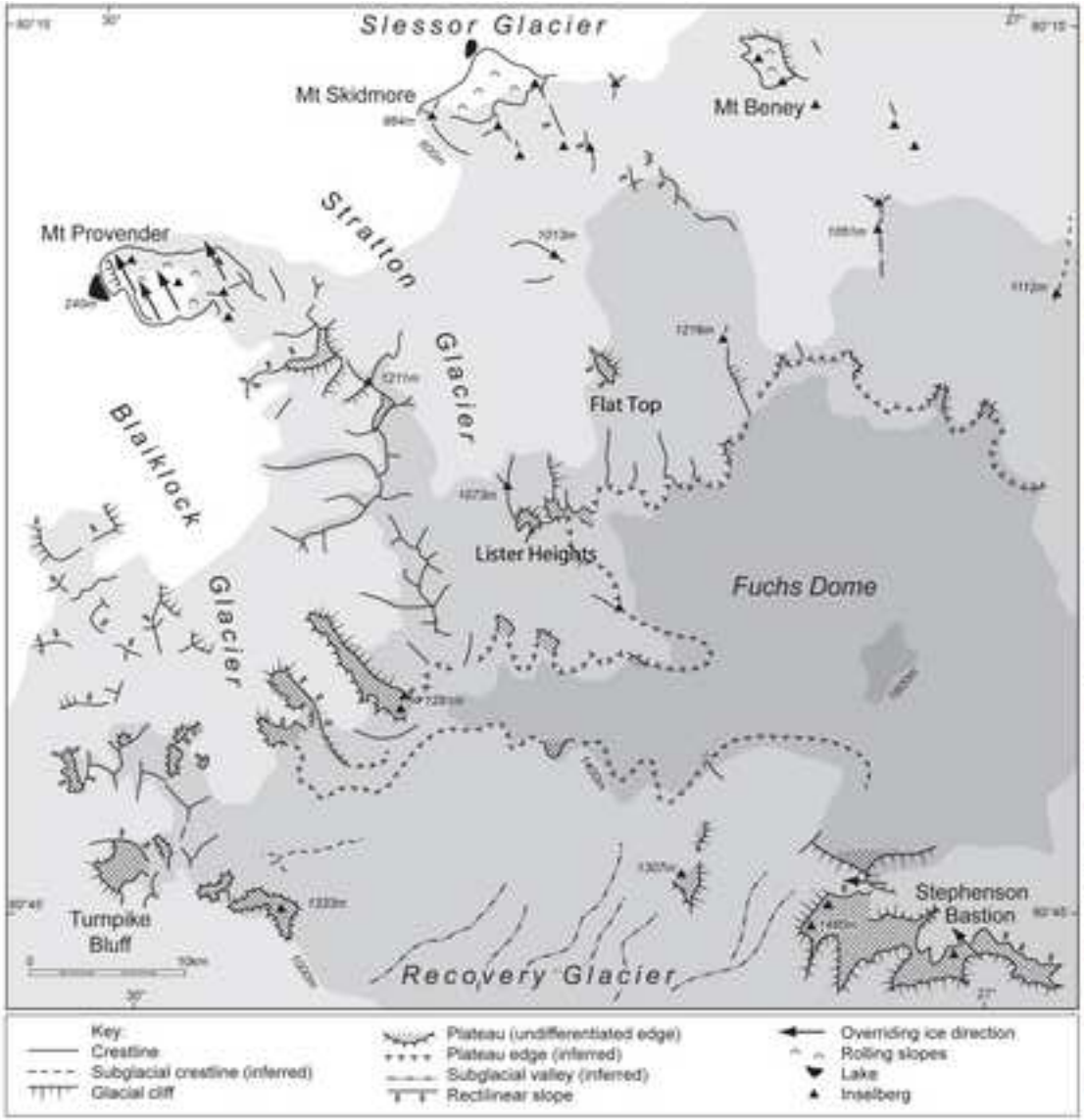

Figure 4a

Click here to download high resolution image

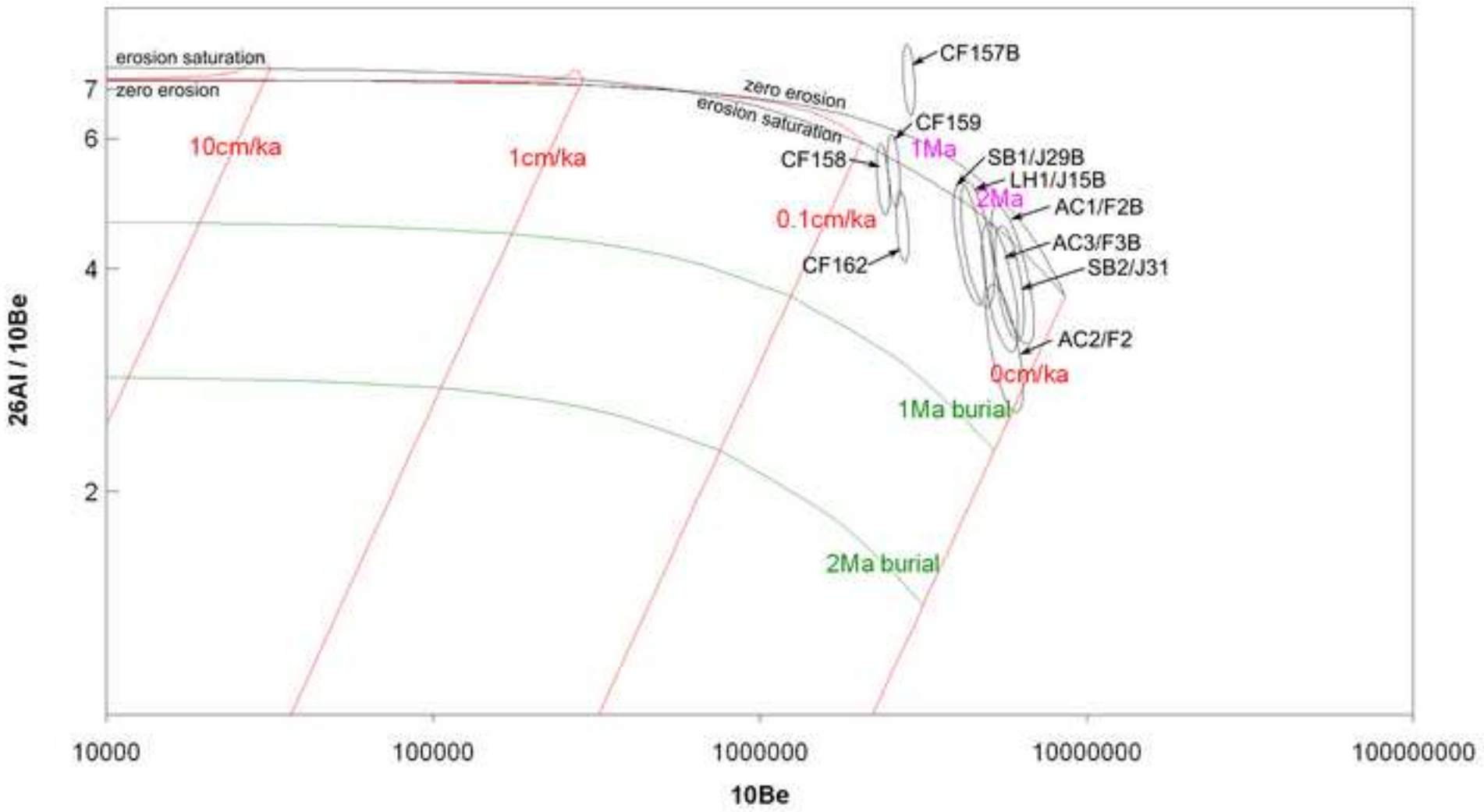

Figure 4b

Click here to download high resolution image

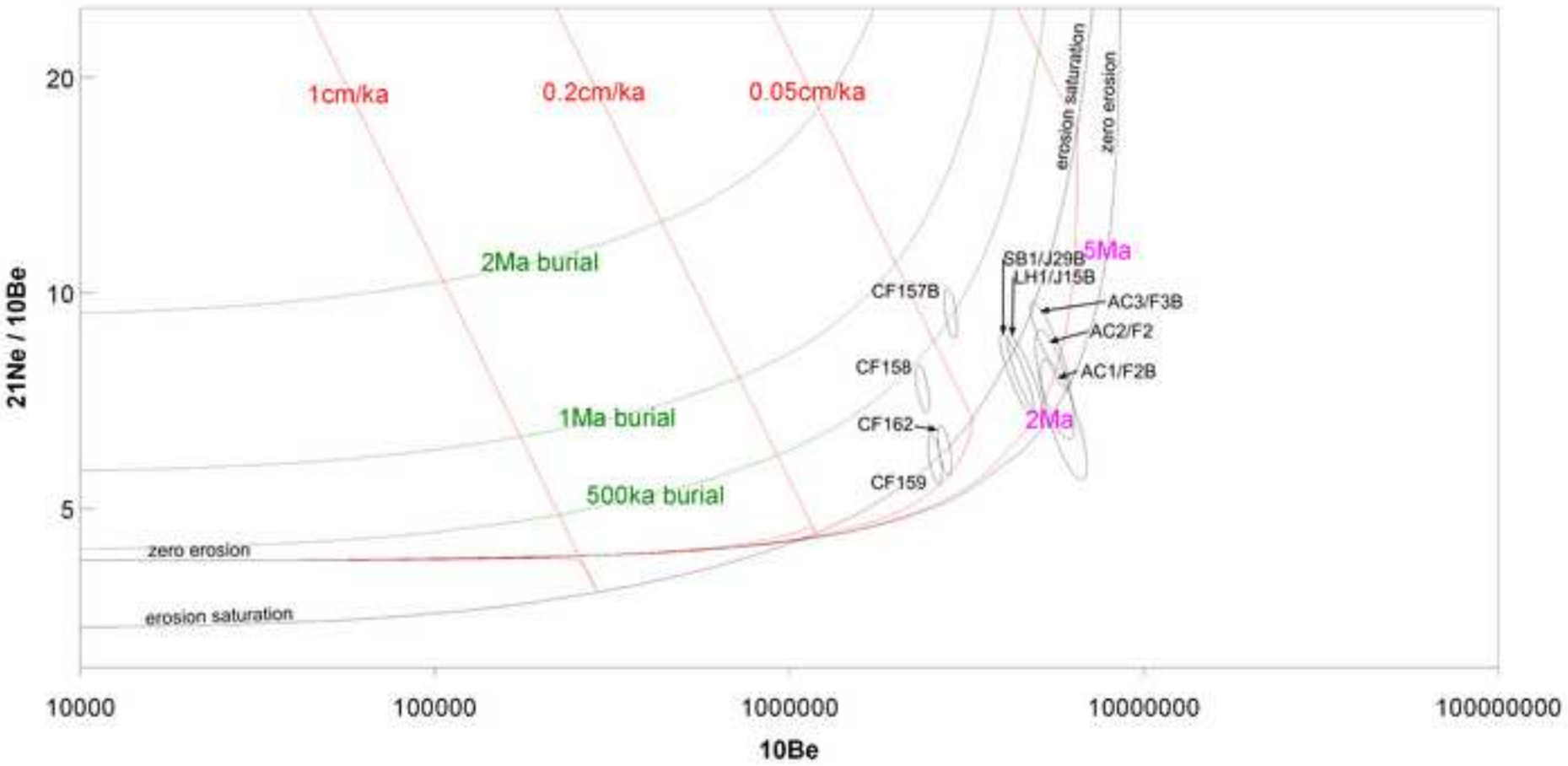

Figure 5 upper

Click here to download high resolution image

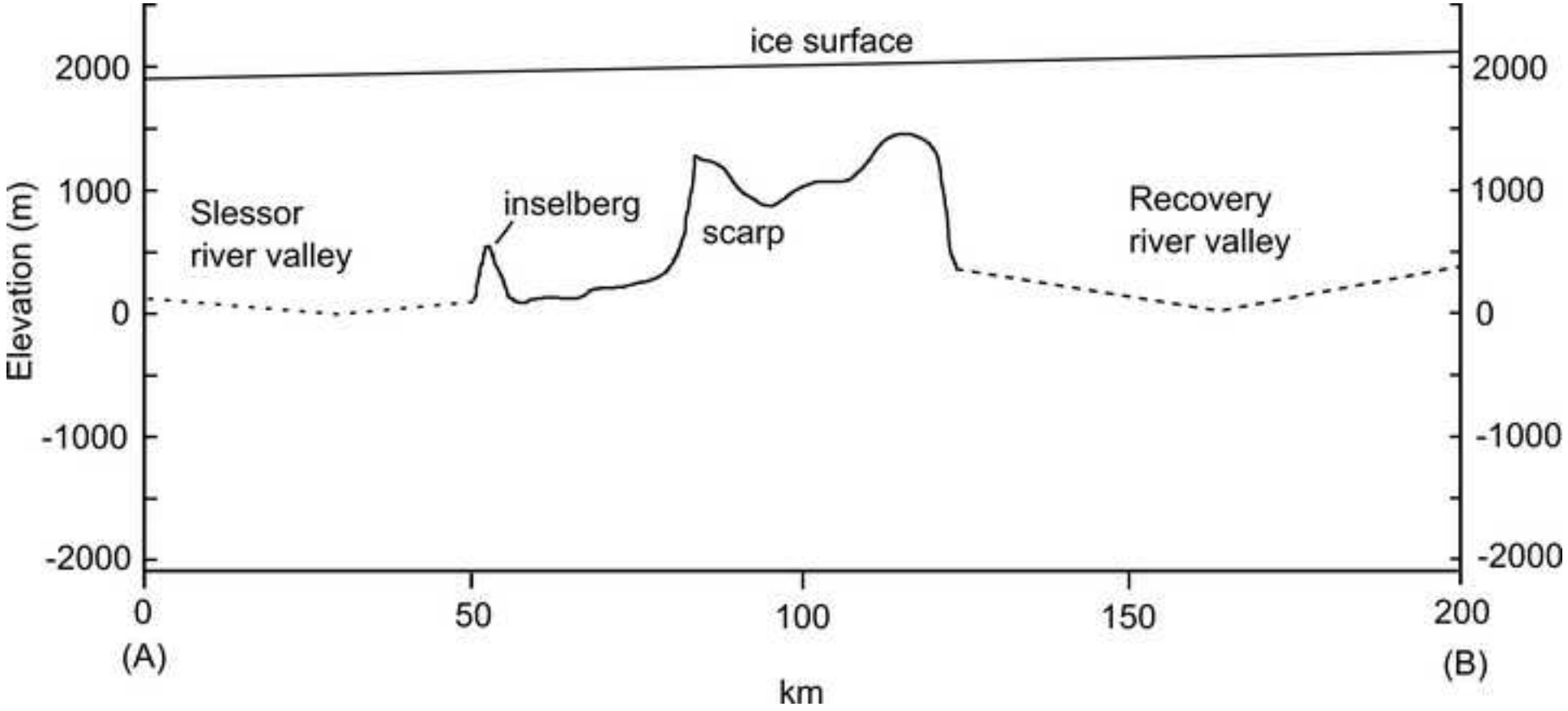

Figure 5 lower

Click here to download high resolution image